Locally Controlled Growth of Individual Lambda-Shaped Carbon Nanofibers

Christian Lutz, Uwe Bog, Tobias Loritz, Julia Syurik, Sharali Malik, Chethala Neelakandhan Shyam Kumar, Christian Kübel, Michael Bruns, Christian Greiner, Michael Hirtz, and Hendrik Hölscher**

The locally defined growth of carbon nanofibers with lambda shape in an open flame process is demonstrated. Via the growth time, the geometry of the structures can be tailored to a Λ- or λ-type shape. Microchannel cantilever spotting and dip-pen nanolithography are utilized for the deposition of catalytic salt $NiCl_2 \cdot 6H_2O$ for locally controlled growth of lambda-shaped carbon nanofibers. Rigorous downscaling reveals a critical catalytic salt volume of 0.033 μm³, resulting in exactly one lambda-shaped carbon nanofiber at a highly predefined position. An empirical model explains the observed growth process.

1. Introduction

Since Zhou and Seraphin published their study of branched carbon nanotubes (CNTs) with L, Y, and T shapes in 1995,[1] various approaches were presented to grow such structures.[2–13] Branched carbon nanotubes are commonly considered of high interest due to their unique electrical properties.[2,3,14] Gothard et al., for example, grew CNTs with Y-junctions by using a mixture of ferrocene, xylene, and a titanium containing vapor.[5] This growth process was used to fabricate Y-shaped CNTs, which were analyzed for their electrical properties.[15] Other options for the defined fabrication include electron beam welding and the growth in molds.[2–4,6]

However, in many cases, the defined growth of branched CNTs is not straightforward because it relies on elaborate process steps. Consequently, in order to understand the growth mechanism of branched nanotubes in more detail, the growth of Y-shaped multiwalled carbon nanotubes (MW-CNTs) or carbon nanofibers (CNFs) is significant, too. Beside their potential use as nanoelectrical devices, branched carbon nanotubes are also of interest as material mimicking hierarchical nanostructures found in nature. Geckos, for example, have hierarchical nanostructures at their toes enabling them to stick and climb on nearly every surface.[16,17] Nonbranched MW-CNTs and CNFs are, due to their size and mechanical properties, already used to mimic nanostructures of geckos.[18–21] Branched CNFs might lift the mimicry to the next hierarchy level improving the overall adhesion on rough surfaces.

In general, the growth of branched or nonbranched CNTs or CNFs needs complex machinery and methods like chemical vapor deposition (CVD) relying on a certain amount of process gases and considerable energy input.[2,6,9,12,22–24] Other approaches like welding of selected CNTs by electron beams are most likely beyond any commercial application.[4] Alternative growth processes utilizing an open flame from a paraffin wax candle,[25] a butane-based Bunsen burner,[26] or an ethanol burner[21,27–30] are less demanding regarding machinery, process gases, and energy input. However, compared to conventional CVD or plasma-enhanced CVD processes, which are widely described in textbooks, they are only sparsely examined up to now. It is a reasonable advantage of such a process that it needs no vacuum and the flame provides the necessary heat and process gases at the same time. Considering the upscaling potential of these methods, it seems highly desirable to have a simple, but precise open flame process, which enables the controlled and facilitated growth of branched CNFs or CNTs.

Here, we present an approach to grow inverted V-shaped or Y-shaped CNFs at highly defined positions in an open ethanol flame. Due to their resemblance to the Greek letter lambda, we named them lambda-shaped CNFs and depending on their

C. Lutz, T. Loritz, Dr. J. Syurik, Dr. H. Hölscher
Institute of Microstructure Technology (IMT) and Karlsruhe Nano Micro Facility (KNMF)
Karlsruhe Institute of Technology (KIT)
Hermann-von-Helmholtz-Platz 1, 76344
Eggenstein-Leopoldshafen, Germany
E-mail: hendrik.hoelscher@kit.edu

Dr. U. Bog, Dr. S. Malik, C. N. S. Kumar, Dr. C. Kübel, Dr. M. Hirtz
Institute of Nanotechnology (INT) and Karlsruhe Nano Micro Facility (KNMF)
Karlsruhe Institute of Technology (KIT)
Hermann-von-Helmholtz-Platz 1, 76344
Eggenstein-Leopoldshafen, Germany
E-mail: michael.hirtz@kit.edu

C. N. S. Kumar
Department of Materials and Earth Sciences
Technische Universität Darmstadt
64287 Darmstadt, Germany

Dr. M. Bruns, Dr. C. Greiner
Institute for Applied Materials (IAM) and Karlsruhe Nano Micro Facility (KNMF)
Karlsruhe Institute of Technology (KIT)
Hermann-von-Helmholz-Platz 1, 76344
Eggenstein-Leopoldshafen, Germany

Dr. C. Greiner
KIT IAM-CMS MikroTribologie Centrum μTC
Strasse am Forum 5, 76131 Karlsruhe, Germany

exact geometry, we use the acronym ΛCNF or λCNF. Λ-shaped CNFs consist of two CNFs attached to the substrate with one of their respective ends and connected to each other through the Ni catalyst, resulting in a freestanding Λ-shape. In the case of λ-shaped CNFs, the two "legs" of the Λ-shaped CNF merge and an additional CNF grows from the junction of the first two CNFs with advancing growth time. In this case, the junction consists of carbon and the nickel catalyst is advanced to the end of the third CNF. The exact growth position of the overall structure on the substrate can be determined though microchannel cantilever spotting (μCS),[31,32] or dip-pen nanolithography (DPN),[33] via locally controlled deposition of catalytic salt $NiCl_2 \cdot 6H_2O$. In this way, by downscaling of this deposition process, we achieved spot sizes that result in the growth of single lambda-shaped CNFs at a predefined position.

2. Results and Discussion

2.1. Setup for CNF Growth in Open Ethanol Flame

Pan and Bao demonstrated growth of CNFs in an open ethanol flame in 2002.[27] Inspired by this and other studies,[25–30] we grew CNFs from $NiCl_2 \cdot 6H_2O$ on silicon substrate completely covered with a thin 60 nm copper layer in an open ethanol flame and studied the adhesion properties of the resulting CNF arrays.[21] Considering the simplicity and cost-effectiveness of this process, it is surprising that it works without the usual reduction step, where the catalyst gets reduced by hydrogen or ammonia gas.[34] In the described open flame process, this reduction step is performed through the thin copper layer.[21] Analyzing this growth process in more detail, we observed that the thickness as well the geometry of the copper layer is important for the growth of CNTs/CNFs. The absence of copper gives no CNTs/CNFs at all, while a significant increase of the thickness of the copper layer to some micrometers prevents the growth of CNTs/CNFs, too.[35] Interestingly, changing the geometry of the copper layer to a bar-type structure (**Figure 1**b) allows for the controlled growth of lambda-shaped CNFs.

Lambda-shaped carbon nanofibers grow if catalytic salt and copper are arranged in the open flame, as schematically shown in Figure 1a. The substrate is vertically aligned in the ethanol flame and the catalytic salt $NiCl_2 \cdot 6H_2O$ is deposited close to a grid-like structure of copper bars. The flame first flows along a structure of copper bars resulting in a partial production of hydrogen,[34] which subsequently reduces the nickel catalyst to a pure state.[36] Together with the hydrocarbon vapor from the ethanol flame, the carbon gets dissolved into the metallic catalyst, resulting in the growth of carbon nanofibers.[36]

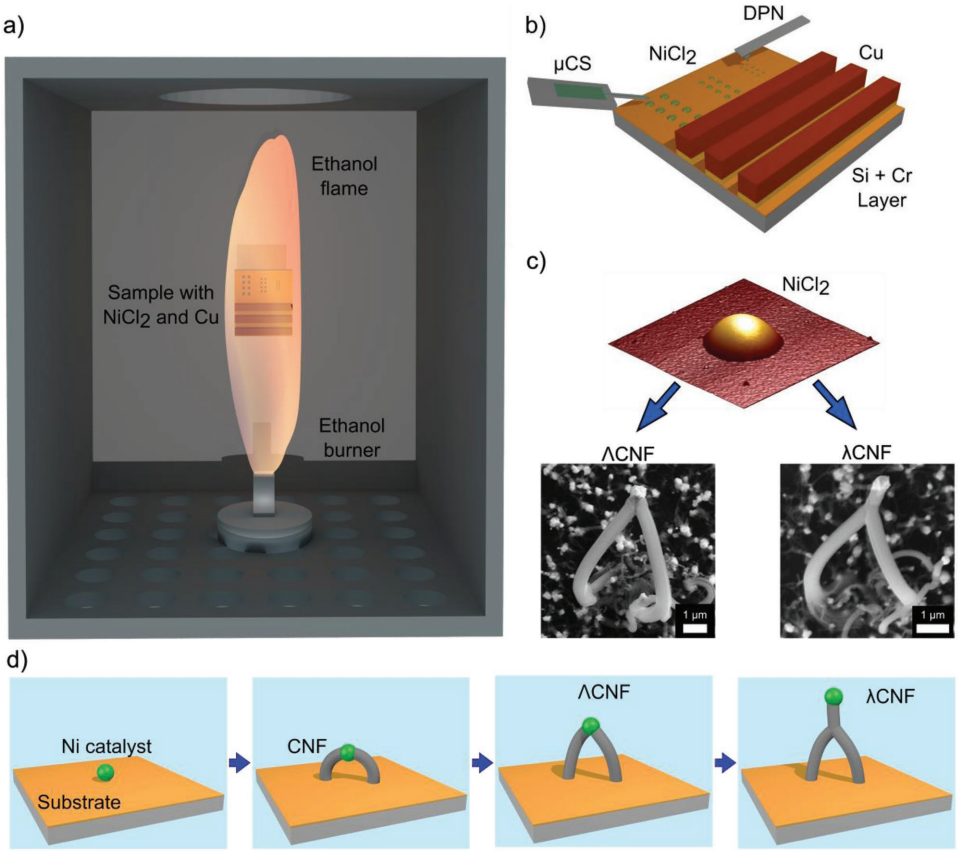

Figure 1. Growing of lambda-shaped CNFs. a) Schematic setup based on an open ethanol flame used for the controlled growth of lambda-shaped CNFs. b) Schematic of the DPN and μCS writing process of the catalytic salt on the substrate. c) AFM topography scans of a dried microspots of catalytic salt. After ethanol flame synthesis, lambda-shaped CNFs grow from such spots. Depending on the growth time, ΛCNFs or λCNFs can be obtained, as shown by the two SEM images. d) Schematic visualizing the growth of lambda-shaped CNFs (not to scale).

In general, the growth of CNTs/CNFs in an open flame is comparably facile. Exposing the silicon substrate, covered with a copper layer of right thickness and a suitable catalytic salt, to the ethanol flame by hand with tweezers is sufficient.[21] For the current study, however, we built a setup allowing for a more controlled growth of lambda-shaped CNFs. Its main feature is a chamber encasing the ethanol flame (see Figure 1a and Figure S3 in the Supporting Information). Small holes in the base plate and a bigger hole in the ceiling plate of the chamber facilitate a constant air flow around the ethanol burner, resulting in a highly laminar ethanol flame, exhibiting no visible turbulence. Such a construction is necessary, because jitter of the flame might expose the sample to ambient conditions for a short time, which would result in oxidation of the nickel catalysts and subsequent stop of CNF growth. The temperature in the center of the sample, where the lambda-shaped CNFs grow, was measured with a thermocouple to 750 °C. As low humidity is an important factor for successful CNF growth,[21] we prepared all samples at a relative humidity below 50% and temperature below 23 °C. Optionally, a magnet can be incorporated into the setup, facilitating an oriented alignment of CNFs during their growth.[21,30] Nonetheless, experiments without magnet result in lambda-shaped CNFs as well. The growth itself is not influenced only the overall orientation of the CNFs.[21]

2.2. Site-Specific CNF Growth

Figure 2 shows the controlled growth of lambda-shaped CNFs from ordered microspots of the catalytic salt $NiCl_2 \cdot 6H_2O$ deposited by µCS. For this, 1.5 µL of a solution containing a concentration of 2 mg mL^{-1} of $NiCl_2 \cdot 6H_2O$ dissolved in ethanol and diluted with glycerol (1:10) was prepared and filled into the reservoir of a microchannel cantilever. As demonstration of process precision, we performed structured writing of microspot arrays. A dwell time of 0.5 s, a relative humidity of 40%, and a spot distance of 20 µm were set for the deposition. The subsequent growth time in the ethanol flame was 10 min. The scanning electron microscopy (SEM) images in Figure 2a reveal the controlled growth of λCNFs directly at the spots, where the catalytic salt was deposited. Gradual zoom-ins show that each single microspot is densely covered with λCNFs. Analyzing their geometry, we observed diameters of the λCNFs in the range of some hundreds of nanometers. The diameters of the two CNFs connected to the substrate's surface are (411.3 ± 76.6) nm ($n = 64$) and are typically slightly smaller as the diameter of the third, freestanding CNF (437.8 ± 68.9) nm ($n = 32$). For the angles between the three branches, the angles between the two CNFs connected with the ground are (101.6 ± 20.0)° ($n = 32$), whereas the other two angles between the third CNF and the two "leg" CNFs are symmetric with (128.4 ± 18.4)° ($n = 64$).

2.3. Chemical Analysis of CNF

For the analysis of the chemical composition of the grown structures, we prepared larger and denser arrays of such microspots (not shown). Raman spectroscopy (Figure 2b) with a 532 nm laser excitation shows the D and G bands at 1356 and 1587 cm^{-1}, respectively. These are characteristics for carbon materials. Figure 2c shows a C 1s XP spectrum from an X-ray photoelectron

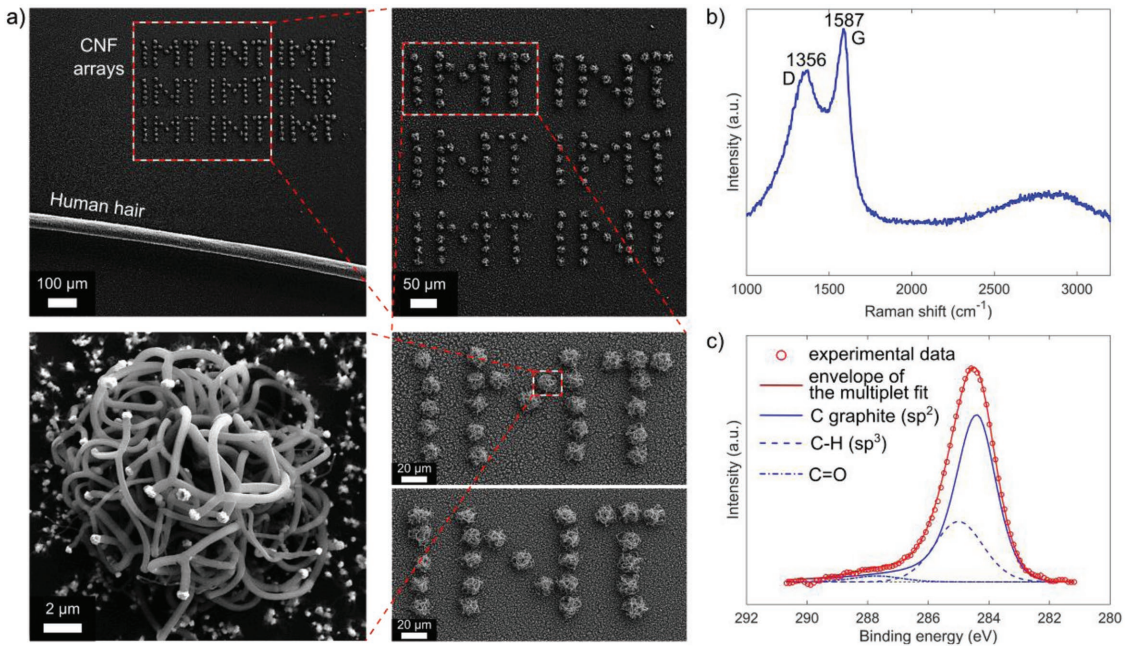

Figure 2. Controlled growth of lambda-shaped CNFs from ordered arrays of catalytic salt $NiCl_2 \cdot 6H_2O$ deposited by µCS. a) For comparison of dimension, a human hair with a diameter of about 80 µm was placed below the logos "IMT" and "INT" representing the two institutes of the KIT involved into this study. A SEM image with higher magnification shows a bunch of λCNFs grown from this spot. b) Raman spectra of such bundles show the D and G bands which are characteristic for carbon materials. c) C 1s XP spectrum of lambda-shaped CNFs, with the experimental data (red circles) and the envelope of the multiplet fit (red solid line). The main component (blue solid line) at a binding energy of 284.4 eV indicates graphite sp^2, whereas the weak component (blue dashed line) at 285.0 eV indicates adventitious carbon sp^3.

spectroscopy (XPS) measurement and compares the experimental data (red circles) with the envelope of the multiplet fit (red solid line). The main component (blue solid line) at a binding energy of 284.4 eV proves graphitic carbon sp^2. The weak component (blue dashed line) at 285.0 eV indicates adventitious carbon sp^3, which most likely originates from the exposure to ambient atmosphere resulting in hydrocarbon contamination.[21]

2.4. Single-CNF Growth Control

To elucidate the growth mechanism of lambda-shaped CNF in more detail, we performed rigorous downscaling of the catalytic salt deposition by applying DPN. At first, a row of five microspots with the same size was produced by using µCS with a dwell time of 2 s and a relative humidity of 60%. Afterward, these microspots acted as reservoirs for loading a DPN tip with catalytic salt solution by aligning the tip to one respective spot and then approaching it toward the surface until it was dipped into it.

With the ink-loaded DPN tip, smaller spots in a subsequent column with a dwell time of 4 s by 60% relative humidity were produced. Such a writing cycle was repeated several times with a distance of 20 µm to the previous spots, resulting in an array of 5 × 10 spots of catalytic salt. Before the subsequent atomic force microscopy (AFM) analysis of the deposited catalytic salt and the following growth in the ethanol flame, the sample was dried for more than 24 h. **Figure 3**a,b shows spots from the first five rows and the last five rows of this depositing process,

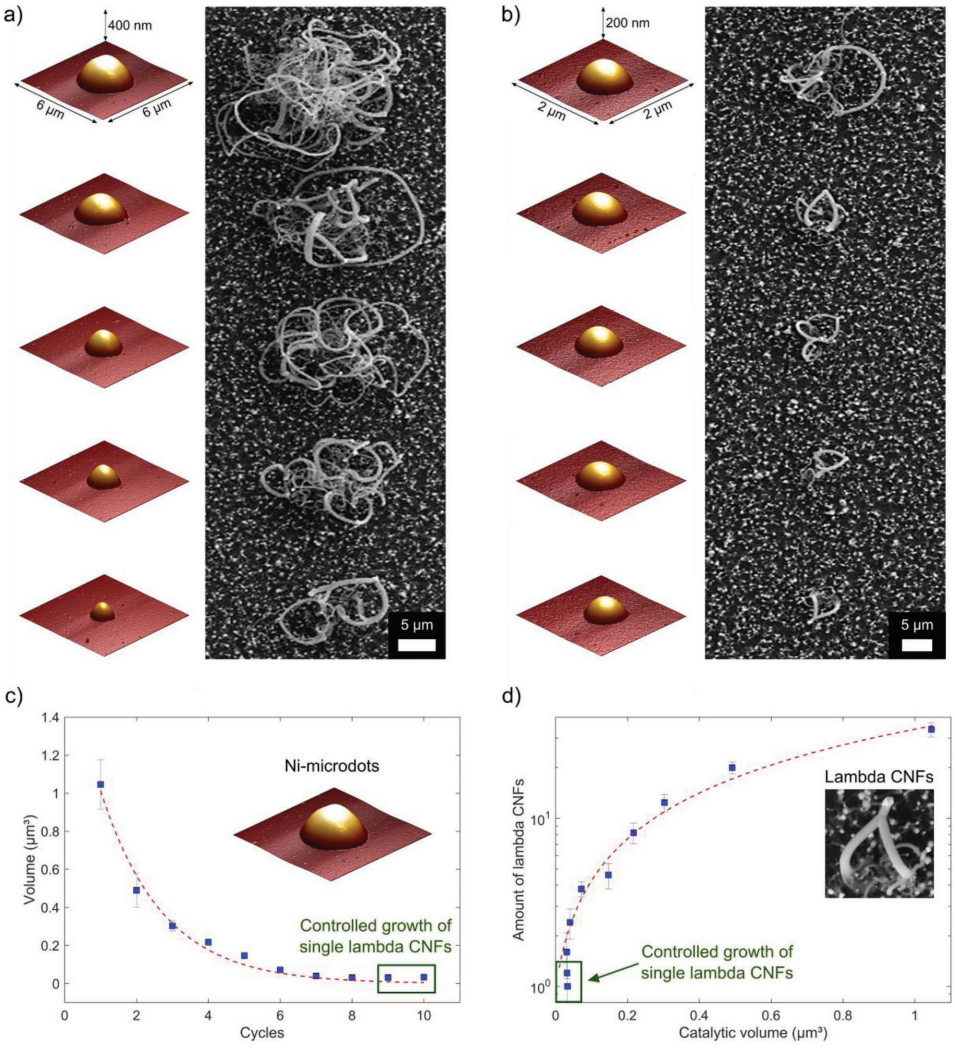

Figure 3. Controlled downscaling of the catalytic salt $NiCl_2 \cdot 6H_2O$ deposition by µCS and DPN in order to obtain single lambda-shaped CNFs. a) 3D AFM images of dried microspots of catalytic salt (left side) and the corresponding lambda-shaped CNFs after growth (right side). The volume of catalytic salt decreases from the first (top) to the fifth (bottom) deposition cycle. b) The same as in (a) but for the sixth to tenth deposition cycle. Please note that the scan field was reduced from 6 × 6 to 2 × 2 µm². For the ninth and tenth deposition cycles, the amount of catalytic salt is so small that only one lambda-shaped CNT grew. c) A plot of the volume of the catalytic salt versus deposition cycle, with the averaged data points (blue squares) and a fit (red dashed line). The fit demonstrates a nearly exponential decline (exponential fit: $V_{Ni}(i) = 1.812e^{-0.5816i}$). d) Correlation of the amount of lambda-shaped CNFs versus the catalytic salt volume. The marked symbols correspond to the growth of single lambda-shaped CNFs. The data points in (c) and (d) are averaged values from five respective deposition spots with the same nominal volume.

respectively. The AFM topography scans on the left show the catalytic salt $NiCl_2 \cdot 6H_2O$ and the corresponding lambda-shaped CNF grown from these spots on the right side. As intended by the applied DPN process, the volume of the catalytic salt spots decreased gradually with each deposition cycle in all columns (please note the change of the scan field between Figure 3a,b).

Figure 3c shows the volume for each DPN deposition cycle calculated from the AFM topography scans containing the respective geometrical information (see the Supporting Information). For the first DPN cycle, an averaged volume (1.05 ± 0.14) μm^3 ($n = 5$) was determined for the catalytic salt. With increasing cycle number, the volume declines nearly exponentially to a volume of (0.0336 ± 0.0081) μm^3 ($n = 5$) for the tenth cycle (see dashed line in Figure 3c). This exponential decline is a well-known phenomenon in DPN and allows for a controlled writing after conditioning of the tip.[37–40]

Exposing this sample to the ethanol flame demonstrates that multiple lambda-shaped CNFs grow from spots with larger volumes of catalytic salt, the number of CNFs decreases with the volume of catalytic salt till only one single lambda-shaped CNF grows. Figure 3d correlates the amount of lambda-shaped CNFs with the volume of the catalytic salt. For that, we counted the number of lambda-shaped CNFs of each microspot by evaluating the corresponding SEM images. Analogous to the catalytic volume, the amount of lambda-shaped CNFs decreases exponentially with the DPN cycles. The critical volume concentration of catalytic salt, required to grow exactly one lambda-shaped CNF, can be deduced from the graph in Figure 3d and is about 0.033 μm^3.

2.5. CNF Growth Mechanism

In addition to the volume of the catalytic salt, the growth time is an important factor to control the growth of lambda-shaped CNFs, as their final shape depends on this parameter (Figure 1c). Growth times of 5 min lead to ΛCNFs (**Figure 4**a), whereas growth times of 10 min result in λCNFs (Figure 4b). These growth times are no strict limits. A minor amount of ΛCNFs might still exists after 10 min since not all CNFs nucleate at the same time. SEM images of structures obtained with various growth times indicate that the nickel catalyst is always at the touching point of the two "legs" of a ΛCNF or the end of the third carbon fiber of a λCNF. Bright-field transmission electron microscopy (BF-TEM) images of the junctions of λCNFs support this assumption (Figure 4c). Practically, all junctions consist only of carbonic material. We observed only a very few examples (<1%) of λCNFs where some remains of the catalysts might be left. This suggests that the third CNF advances with the Ni catalyst from the touching point of the two legs, leaving no catalytic material in the intersection.

Furthermore, energy dispersive X-ray spectroscopy (EDX) experiments were performed to investigate the material composition on different parts of the lambda-shaped CNFs (Table S1, Supporting Information). The body of the CNF and the junction has nearly the same material composition with about 64–65 wt% carbon and residual amounts of oxygen, silicon, and copper. The catalytic centers consist of carbon, oxygen, silicon, and a nickel/copper alloy (1:20). This indicates the importance of copper for the growth of lambda-shaped CNFs. The detected silicon signal originates—at least in part—from the used growth substrate.

However, the lambda-shaped CNFs presented so far grow on a substrate where some remains of Cr might be present. The 7 nm thick chromium served as adhesion layer during the lithography process. We, therefore, conducted some experiments with substrates containing no Cr at all. As shown in Figure S5 (Supporting Information), lambda-shaped CNFs grow also on a substrate layered with SiO_2, Au, and Cu as long as copper is provided through the open flame process.

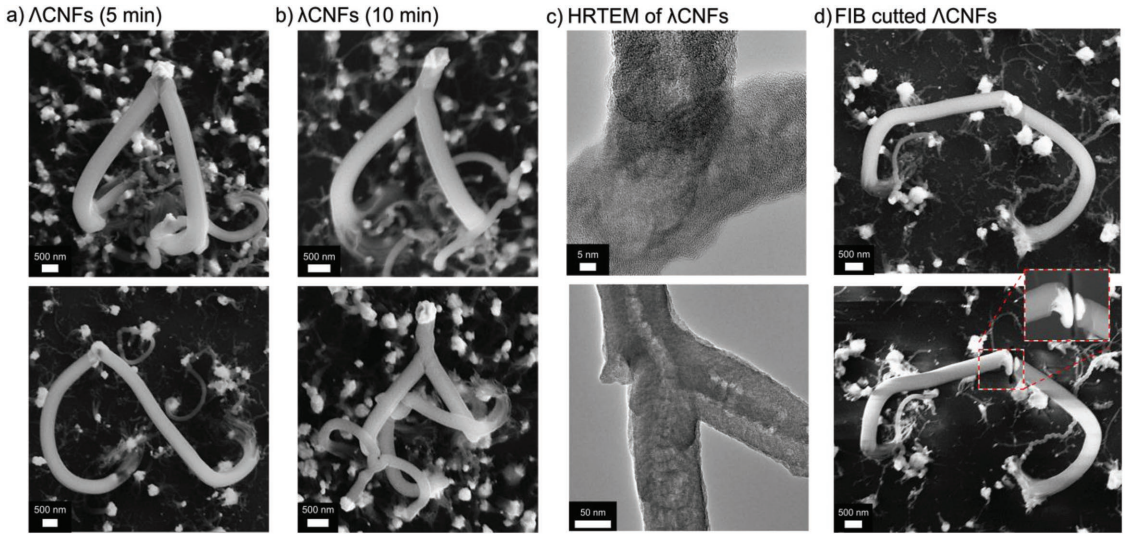

Figure 4. Examples of lambda-shaped CNFs grown from tiny microspots of $NiCl_2 \cdot 6H_2O$ with a concentration of 2 mg mL^{-1} and a volume of about 0.033 μm^3 placed via DPN on the sample surface. a) SEM images of ΛCNF after growth times of 5 min. b) Increasing the growth time leads to λCNFs. These samples grow after 10 min. The catalytic centers are visible as bright particles at the ends of the lambda-shaped CNFs and consist presumably of nickel. c) BF-TEM images of junctions of λCNFs of different sizes show no parts of catalytic (i.e., metallic) material in the junctions. d) SEM images of lambda-shaped CNFs before (top) and after a cut (bottom) with a focused ion beam. A ΛCNF before and after a cut through the catalytic center is displayed on top and bottom, respectively. The overall shape of the two CNF "legs" does not change after this procedure, indicating that there is no internal stress in the structure.

Based on these results, we considered two different models for the growth process of the lambda-shaped CNFs. One model might be that the two "legs" grow independently from each other from two closely neighbored Ni catalysts. Since the two CNFs are exposed to thermal fluctuations during growth in the ethanol flame, the two "legs" will oscillate randomly and the two nickel catalysts eventually touch each other. As a result, the two Ni catalysts might fuse forming a ΛCNF from which a third CNF grows upward, resulting in the presented λCNF. However, some of our observations speak against this independent growth model. First, we observed that the two "legs" of any lambda-shaped CNF always have approximately same length and diameter. Second, even in dense bundles of lambda-shaped CNFs (see Figure 2a), it seems that each CNF finds exactly one partner and we never observed two independent CNFs shortly before touching in such a crowd of lambda-shaped CNFs. Finally, if the two "legs" grow independently and merge accidentally through thermal activation, there should be internal stress in the structure. However, after cutting lambda-shaped CNFs with a focused ion beam (FIB), we observed no change of shape as demonstrated by the SEM images (Figure 4d) of a ΛCNF before and after cutting its catalytic center into two parts. This result is a strong indication that no residual stress is present in the nanostructure.

Consequently, we conclude that lambda-shaped CNFs grow as depicted in Figure 1d and Figure S4 (Supporting Information). At first $NiCl_2 \cdot 6H_2O$ is reduced to Ni catalyst in the ethanol flame. Tiny microspots (as deposited by DPN) result in single Ni-catalytic particles, while larger microspots (as deposited by μCS) break up into several Ni-catalyst particles during growth in the ethanol flame. Two nearly identical CNFs grow from each single Ni-catalyst particle. Subsequently, the two CNFs anchor with the substrate. The tension between the two elongating "legs" initiates the buildup of an arc, resulting in a ΛCNF after short time. After establishing of the ΛCNF, the two CNFs will touch each other underneath the Ni-catalyst particle after some time. As a result, the Ni-catalyst particle grows upward, resulting in a λCNF.

3. Conclusion

In conclusion, we presented an open ethanol flame method for the growth of a new kind of CNFs, which we call lambda-shaped CNFs. The lambda-shaped CNFs reveal Λ or λ shapes, which can be controlled via the growth time. Growth times of about 5 min lead to Λ-shaped CNFs, whereas longer growth times of about 10 min lead to λ-shaped CNFs. Ordered arrays of lambda-shaped CNFs can be grown by controlled deposition of $NiCl_2 \cdot 6H_2O$ catalytic salt via μCS. Downscaling was performed with μCS and DPN in order to explore the critical volume necessary to grow single lambda-shaped CNFs (0.033 μm³ of $NiCl_2 \cdot 6H_2O$). Even single lambda-shaped CNFs, precisely placed at a desired position, can be grown in this way.

The presented process provides several options for upscaling. The ethanol flame could be easily enlarged, the copper could be integrated into the flame flow as a mesh or powder, the catalytic salt could be deposited with various lithographic procedures. Downsizing of the microspots of catalytic salt to nanoscale spots which might allow for the growth of smaller – or even single-walled – carbon nanotubes will be the task of forthcoming studies.

4. Experimental Section

Substrate Fabrication: For the lambda-shaped CNF growth, a substrate partially covered with arrays of copper grids was fabricated (Figure S1, Supporting Information). The base material consisted of a small piece of silicon (1 × 1 cm²) with 1 μm SiO_2 on top. After the evaporation of 7 nm Cr and 50 nm Au, a photoresist (AZ 4533, Microchemicals GmbH, Germany) was spin-coated on the top of the Au layer. Afterward, UV lithography with a mask containing arrays of grids was applied (Figure S2, Supporting Information). After that, the resist was developed to obtain the cavities, which were subsequently filled with copper by a galvano-shaping process. In the final step, the resist was stripped and the Cr/Au layers were etched away (Oxford Instruments Ionfab 300, RIBE, 600 W, 1 min, Ar plasma). The described procedure resulted in a microstructured substrate with a SiO_2 surface partially covered with grids of copper bars with a height of 3 μm, a width of 14 μm, and a periodicity of 60 μm (see SEM in Figure S2 in the Supporting Information).

Deposition of Catalysts: DPN and μCS were performed with a NLP 2000 system (NanoInk Inc., USA). For μCS, a SPT-C10S cantilever from Bioforce Nanosciences (SPT-probes, surface patterning tool),[41] and for DPN, a cantilever type A from NanoInk were used. Deposition was performed directly on the substrate about 50 μm away from a copper grid. The ink was a solution (2 mg mL^{-1}) of the catalytic salt $NiCl_2 \cdot 6H_2O$ in ethanol mixed with glycerol (1:10).

Growth of Lambda-Shaped CNFs: A self-built setup shown in Figure S3 (Supporting Information) was used to grow lambda-shaped CNFs.[42] It consisted of a chamber with an integrated ethanol burner with a wick of 12 mm width and 2 mm thickness. Its combustion rate was 0.4 mL min^{-1}. The design of the chamber enabled a continuous and stable flow of the ethanol flame without jitter. A perforated nitrogen pipe was circularly placed around the ethanol burner for flooding the spatial area of the ethanol flame with N_2 after the CNF growth to extinguish the flame in a controlled way. Furthermore, the nitrogen flow prevented the exposure of the still hot sample to ambient conditions. The 10 × 10 mm² substrates for the growth of lambda-shaped CNFs were placed vertically over the wick of the ethanol burner at a distance of 2 mm measured from the lower edge of the sample. The CNFs were grown in the middle of the sample, i.e., about 7 mm over the wick. A N52 neodymium block magnet was integrated into the setup during growth, resulting in a calculated magnetic flux of 50 mT at the sample position. As discussed elsewhere, the magnet had no influence on the growth itself but helped to orient the growth direction.[21]

CNF Characterization: The morphology of the lambda-shaped CNFs was investigated by scanning electron microscopy (Zeiss SUPRA 60 VP). TEM of the junction of the lambda-shaped CNFs was performed with a Titan 80-300 (FEI Company) at 80 kV operation voltage. Images were taken with a Gatan US1000 charge-coupled device camera. Raman spectroscopy was performed with a Renishaw inVia Raman microscope at an excitation wavelength of 532 nm. The $NiCl_2 \cdot 6H_2O$ catalytic microspots deposited by μCS and DPN were imaged by AFM (Bruker Dimension Icon) in tapping mode. Size and volume of the microspots were calculated, as described in the Supporting Information. XPS measurements were performed using a K-Alpha + XPS instrument from Thermo Fisher Scientific using the Thermo Avantage software for data acquisition and processing. The arrays with lambda-shaped CNFs were investigated by using a microfocused monochromated Al Kα X-ray source with a spot size of 30–400 μm. Spectra were fitted by using Voigt profiles and the spectra were referenced to the C 1s hydrocarbon peak at 285.0 eV. EDX measurements were performed with a Zeiss Leo 1530 SEM operating at 20 kV. The EDX was acquired using the "Point & ID" option in INCA software using an Oxford X-MaxN 50 detector.

FIB Cutting of CNFs: Some lambda-shaped CNFs were cut using a focused ion beam (Helios Nanolab 650 from FEI) operating at an acceleration voltage of 30 kV with an ion beam current of 40–80 pA. The cutting time was 1 s for the cut between the nickel catalysts of ΛCNFs (see Figure 4d).

Supporting Information

Supporting Information is available from the Wiley Online Library or from the author.

Acknowledgements

It is a pleasure for the authors to thank Richard Thelen for engineering advice to build the setup to grow lambda-shaped CNFs and Moaaz Nizami and Markus Guttmann for their kind support in the lab. Furthermore, the authors thank the IMT clean room team for the kind manufacturing of the sample substrates. J.S. gratefully acknowledges funding from the Helmholtz Postdoc Programme (PD-157). S.M. acknowledges support by the Helmholtz Society through the program Science and Technology (STN). J.S. and M.H. thank the Young Investigator Network (YIN) for financial support through a YIN grant award. The K-Alpha + instrument was financially supported by the Federal Ministry of Economics and Technology on the basis of a decision by the German Bundestag. This work was partly carried out with the support of the Karlsruhe Nano Micro Facility (KNMF, www.kit.edu/knmf), a Helmholtz Research Infrastructure at Karlsruhe Institute of Technology (KIT, www.kit.edu).

Conflict of Interest

The authors declare no conflict of interest.

Keywords

branched carbon nanofibers, dip-pen nanolithography (DPN), lambda-shaped carbon nanofibers, microchannel cantilever spotting (μCS)

[1] D. Zhou, S. Seraphin, *Chem. Phys. Lett.* **1995**, *238*, 286.
[2] J. Li, C. Papadopoulos, J. Xu, *Nature* **1999**, *402*, 253.
[3] C. Papadopoulos, A. Rakitin, J. Li, A. S. Vedeneev, J. M. Xu, *Phys. Rev. Lett.* **2000**, *85*, 3476.
[4] M. Terrones, F. Banhart, N. Grobert, J. C. Charlier, H. Terrones, P. M. Ajayan, *Phys. Rev. Lett.* **2002**, *89*, 5.
[5] N. Gothard, C. Daraio, J. Gaillard, R. Zidan, S. Jin, A. M. Rao, *Nano Lett.* **2004**, *4*, 213.
[6] G. Meng, Y. J. Jung, A. Cao, R. Vajtai, P. M. Ajayan, *Proc. Natl. Acad. Sci. USA* **2005**, *102*, 7074.
[7] Y. C. Choi, W. Choi, *Carbon* **2005**, *43*, 2737.
[8] O. T. Heyning, P. Bernier, M. Glerup, *Chem. Phys. Lett.* **2005**, *409*, 43.
[9] D. Wie, Y. Liu, L. Cao, L. Fu, X. Li, Y. Wang, G. Yu, D. Zhu, *Nano Lett.* **2006**, *6*, 186.
[10] Q. Liu, W. Liu, Z. M. Cui, W. G. Song, L. J. Wan, *Carbon* **2007**, *45*, 268.
[11] J. Huang, D. H. Kim, R. Seelaboyina, B. K. Rao, D. Wang, M. Park, W. B. Choi, *Diamond Relat. Mater.* **2007**, *16*, 1524.
[12] E. X. Ding, J. Wang, H. Z. Geng, W. Y. Wang, Y. Wang, Z. C. Zhang, Z. J. Luo, H. J. Yang, C. X. Zou, J. Kang, L. Paet, *Sci. Rep.* **2015**, *5*, 11281.
[13] S. Malik, Y. Nemoto, H. Guo, K. Ariga, J. P. Hill, *Beilstein J. Nanotechnol.* **2016**, *7*, 1260.
[14] M. Menon, D. Srivastava, *Phys. Rev. Lett.* **1997**, *79*, 4453.
[15] P. R. Bandaru, C. Daraio, S. Jin, A. M. Rao, *Nat. Mater.* **2005**, *4*, 663.
[16] K. Autumn, Y. A. Liang, S. T. Hsieh, W. Zesch, W. P. Chan, T. W. Kenny, R. Fearing, R. J. Full, *Nature* **2000**, *405*, 681.
[17] K. Autumn, P. H. Niewiarowski, J. B. Puthoff, *Annu. Rev. Ecol., Evol., Syst.* **2014**, *45*, 445.
[18] B. Yurdumakan, N. R. Raravikar, P. M. Ajayan, A. Dhinojwala, *Chem. Commun.* **2005**, 3799.
[19] Y. Zhao, T. Tong, L. Delzeit, A. Kashani, M. Meyyappan, A. Majumdar, *J. Vac. Sci. Technol., B: Microelectron. Nanometer Struct.* **2006**, *24*, 331.
[20] L. Qu, L. Dai, M. Stone, Z. Xia, Z. L. Wang, *Science* **2008**, *322*, 238.
[21] C. Lutz, J. Syurik, C. N. S. Kumar, C. Kübel, M. Bruns, H. Hölscher, *Beilstein J. Nanotechnol.* **2017**, *8*, 2719.
[22] M. F. L. De Volder, S. H. Tawfick, R. H. Baughman, A. J. Hart, *Science* **2013**, *339*, 535.
[23] A. Cao, R. Baskaran, M. J. Frederick, K. Turner, P. M. Ajayan, G. Ramanath, *Adv. Mater.* **2003**, *15*, 1105.
[24] Z. Zhang, B. Wei, J. W. Ward, R. Vajtai, G. Ramanath, P. M. Ajayan, *Adv. Mater.* **2001**, *13*, 1767.
[25] Y. Y. Li, C. C. Hsieh, *Micro Nano Lett.* **2007**, *2*, 63.
[26] C. Hsieh, M. Youh, H. Wu, L. Hsu, J. Guo, Y. Li, *J. Phys. Chem. C* **2008**, *112*, 19224.
[27] C. Pan, Q. Bao, *J. Mater. Sci. Lett.* **2002**, *21*, 1927.
[28] C. Pan, Y. Liu, F. Cao, J. Wang, Y. Ren, *Micron* **2004**, *35*, 461.
[29] Q. Bao, C. Pan, *Nanotechnology* **2006**, *17*, 1016.
[30] J. Zhang, C. Pan, *J. Phys. Chem. C* **2008**, *112*, 13470.
[31] M. Hirtz, A. M. Greiner, T. Landmann, M. Bastmeyer, H. Fuchs, *Adv. Mater. Interfaces* **2014**, *1*, 1300129.
[32] J. Atwater, D. S. Mattes, B. Streit, C. von Bojničić-Kninski, F. F. Loeffler, F. Breitling, H. Fuchs, M. Hirtz, *Adv. Mater.* **2018**, *30*, 1801632.
[33] R. D. Piner, J. Zhu, F. Xu, S. Hong, C. A. Mirkin, *Science* **1999**, *283*, 661.
[34] A. Kumar, A. Cross, K. Manukyan, R. R. Bhosale, L. J. P. van den Broeke, J. T. Miller, A. S. Mukasyan, E. E. Wolf, *Chem. Eng. J.* **2015**, *278*, 46.
[35] B. Gan, J. Ahn, Q. Zhang, Rusli, S. F. Yoon, J. Yu, Q.-F. Huang, K. Chew, V. A. Ligatchev, X.-B. Zhang, W.-Z. Li, *Chem. Phys. Lett.* **2001**, *333*, 23.
[36] M. Kumar, in *Carbon Nanotube Synthesis and Growth Mechanism*, 1st ed. (Ed: S. Yellampalli), InTech, London, UK **2011**.
[37] S. Biswas, M. Hirtz, H. Fuchs, *Small* **2011**, *7*, 2081.
[38] N. Farmakidis, K. A. Brown, *Langmuir* **2017**, *33*, 5173.
[39] A. Förste, M. Pfirrmann, J. Sachs, R. Gröger, S. Walheim, F. Brinkmann, M. Hirtz, H. Fuchs, T. Schimmel, *Nanotechnology* **2015**, *26*, 175303.
[40] T. H. Wu, H. H. Lu, C. W. Lin, *Langmuir* **2012**, *28*, 14509.
[41] J. Xu, M. Lynch, J. L. Huff, C. Mosher, S. Vengasandra, G. Ding, E. Henderson, *Biomed. Microdevices* **2004**, *6*, 117.
[42] T. Loritz, *Master Thesis*, Karlsruhe Institute of Technology (KIT) **2017**.